

# RSC Advances



This is an *Accepted Manuscript*, which has been through the Royal Society of Chemistry peer review process and has been accepted for publication.

*Accepted Manuscripts* are published online shortly after acceptance, before technical editing, formatting and proof reading. Using this free service, authors can make their results available to the community, in citable form, before we publish the edited article. This *Accepted Manuscript* will be replaced by the edited, formatted and paginated article as soon as this is available.

You can find more information about *Accepted Manuscripts* in the [Information for Authors](#).

Please note that technical editing may introduce minor changes to the text and/or graphics, which may alter content. The journal's standard [Terms & Conditions](#) and the [Ethical guidelines](#) still apply. In no event shall the Royal Society of Chemistry be held responsible for any errors or omissions in this *Accepted Manuscript* or any consequences arising from the use of any information it contains.



## Nanostructured cobalt phosphide-based films as bifunctional electrocatalysts for overall water splitting †

Received 00th Month 20xx,  
Accepted 00th Month 20xx

Julian A. Vigil and Timothy N. Lambert\*

DOI: 10.1039/x0xx00000x

www.rsc.org/

**Nanostructured cobalt phosphide-based films were prepared using a simple, three-step electrodeposition-thermal annealing-phosphidation method. The films are effective electrocatalysts for the hydrogen evolution reaction in acidic and alkaline electrolytes, and the oxygen evolution reaction in alkaline electrolyte. A symmetrical alkaline electrolysis cell with low overpotential of 0.41-0.51 V was demonstrated.**

Hydrogen is regarded as a valuable high energy density, zero-emission fuel for the future, with the potential to reduce or eliminate fossil fuels. H<sub>2</sub> also has potential as an energy carrier or storage molecule: i.e. being generated, stored, and consumed to bridge the gap of high and low production cycles of renewable energy sources, such as solar cells and wind turbines. However, H<sub>2</sub> gas is currently manufactured by steam reforming hydrocarbons and methanol oxidation, which produce CO<sub>2</sub>, a greenhouse gas. Water electrolysis<sup>1</sup> and artificial photosynthesis<sup>2</sup> are thus being investigated as clean methods for hydrogen generation.

Water electrolysis, or water splitting, consists of two half-reactions: the cathodic hydrogen evolution reaction (HER) and the anodic oxygen evolution reaction (OER). Both of these reactions contribute to the overall efficiency of water electrolysis. While the thermodynamic potential difference between the HER and the OER is 1.23 V, high overpotentials are typically required due to inherently slow reaction kinetics as a result of electrical, transport, and electrochemical reaction resistances.<sup>3</sup> For example, commercial electrolyzers typically operate at 1.8-2.0 V.<sup>1</sup> Renewable energy technologies such as electrolyzers (and also reversible fuel cells<sup>3</sup> and solar fuel cells<sup>4</sup>) could benefit from the identification of a single catalyst that can perform both the HER and the OER. A bifunctional electrocatalyst with the ability to catalyze both the HER and OER could also simplify electrolyzer design and increase their efficiency.

Platinum group metals are known to be active and generally

stable electrocatalysts, but their high cost and rarity limit their practicality in next-generation devices. Ru- and Ir-based catalysts are best for catalyzing the OER, while Pt-based catalysts are best for the HER. However, none of these metals are highly active for both of these reactions. Recent efforts to develop nanostructured materials have closed the activity gap between precious and non-precious metal electrocatalysts.<sup>5</sup> Nanoscale particles and structures are associated with an increase in surface area, the number of active catalytic sites, and more facile ion and electron transport.

Cobalt has been studied extensively as an electrocatalyst for hydrogen and oxygen electrochemistry relating to energy devices, most notably phosphides and sulfides for the HER<sup>6-7</sup> and hydroxides and oxides for the oxygen reduction reaction (ORR) and OER.<sup>8</sup> Furthermore, it was one of the first transition metals studied for its bifunctional electrocatalytic properties for overall water splitting. The first was a cobalt oxide/hydroxide film reported by Cobo *et al.*,<sup>9</sup> however this catalyst was more accurately described as switchable, as the H<sub>2</sub> and O<sub>2</sub> catalysts were different, but interconvertible by electrochemical modification. A catalyst with both HER and OER activity in its "as-prepared" state would benefit from not requiring further activation or modification. Only recently have such cobalt-based catalysts been identified: a Co nanoparticle/N-doped carbon composite,<sup>10</sup> a Co corrole complex,<sup>11</sup> a Co-Co oxide/N-doped carbon composite,<sup>12</sup> a Co<sub>3</sub>O<sub>4</sub> nanocrystal/carbon fiber composite,<sup>13</sup> a Co phosphide/phosphate film from anodized Co,<sup>14</sup> a Co phosphide/phosphate film from electrodeposited Co and P,<sup>15</sup> a Li-modified CoO/carbon fiber paper composite,<sup>16</sup> and a Co sulfide/Mo disulfide composite.<sup>17</sup> The need for development and understanding in this area cannot be understated; as the few listed systems are the only Co-based bifunctional HER-OER bifunctional catalysts, all reported in only the last several years.

Cobalt phosphide/phosphate films have been pursued on multiple occasions for a few key reasons. First, they are known to be active for the HER and OER with no conductive support, i.e. no carbon incorporation is necessary, which avoids the possibility of carbon corrosion at high OER potentials. Second, the preparation of a cobalt phosphide (or any transition metal phosphide) is a simple, well-known synthetic method that is easily adaptable to multiple precursors (Co<sup>0</sup>, Co<sub>x</sub>O<sub>y</sub>, etc.) and material forms (free powder, films

Department of Materials, Devices & Energy Technologies, Sandia National Laboratories, Albuquerque, New Mexico, 87185, USA, \*Fax: 505 844 7786; Tel: 505 284 6967; E-mail: [tnlambe@sandia.gov](mailto:tnlambe@sandia.gov).

† Electronic Supplementary Information (ESI) available: [General synthetic methods along with additional spectra and data as described within the text]. See DOI: 10.1039/x0xx00000x

etc.). With this in mind, we report the conversion of a nanostructured  $\text{Co}_3\text{O}_4$  film (from electrodeposited  $\text{Co}(\text{NO}_3)_x(\text{OH})_{2-x}\cdot y(\text{H}_2\text{O})$  films<sup>8</sup>) to a CoP film under inert conditions. The subsequent partial surface oxidation under reintroduction to ambient air results in phosphate formation and ultimately a mixed cobalt phosphide/phosphate film, the active material for bifunctional HER-OER electrocatalysis.

The high surface area, nanostructured cobalt phosphide/phosphate films (hereby termed Co-PP) were prepared using a three-step electrodeposition-thermal annealing-phosphidation process. The Co-PP films show low overpotentials, small Tafel slopes, and excellent stability in acidic and alkaline electrolytes for the HER. The films compare favorably to literature HER-OER bifunctional electrocatalysts and to the commercial benchmark, 20% Pt/C. Additionally, the films show low overpotentials and excellent stability for the OER. As a demonstration of this bifunctional nature, water electrolysis with Co-PP electrocatalysts at both the anode and cathode is shown. The overpotential is among the lowest of the few reported symmetrical electrolysis cells.

The synthesis of nanostructured Co-PP films on several substrate foils (Ni, Ti, Au<sup>†</sup>) was achieved using a simple, three-step electrodeposition-thermal annealing-phosphidation approach, as depicted in the schematic in Fig. 1a<sup>†</sup> and further described in the Electronic Supplemental Information (ESI<sup>†</sup>). Building on our previous work,<sup>8</sup> a  $\text{Co}(\text{NO}_3)_x(\text{OH})_{2-x}\cdot y(\text{H}_2\text{O})$  nanostructured film was first electrochemically deposited from an aqueous/alcoholic solution of  $\text{Co}(\text{NO}_3)_3\cdot 6(\text{H}_2\text{O})$  in 0.076 M  $\text{NaNO}_3$ . The cobalt hydroxide film was then heated at 300 °C in air to convert it to spinel  $\text{Co}_3\text{O}_4$ . The spinel cobalt oxide film was then reacted with phosphine gas ( $\text{PH}_3$ ),<sup>14, 18-23</sup> prepared from the *in situ* decomposition of  $\text{NaH}_2\text{PO}_2\cdot(\text{H}_2\text{O})$ , at 300 °C in an inert atmosphere<sup>24</sup> using a simple crucible-based apparatus as shown in Fig. S1 (ESI<sup>†</sup>). Reintroduction of the CoP films in to ambient air resulted in the partial surface oxidation and formation of the Co-PP catalyst. The Co-PP film catalyst loadings were 28  $\mu\text{g}$  total, or 143  $\mu\text{g cm}^{-2}$  when scaled for the electrode's geometric area. Control 20% Pt/C films were also prepared at the same loading for electrocatalytic comparison. Ni, Ti and Au<sup>†</sup> substrates were utilized in order to evaluate possible substrate effects on the electrocatalysis, and demonstrate the generality of the synthetic method.

The formation of a nanostructured, high surface area Co-PP film was verified using scanning electron microscopy (SEM), cyclic voltammetry (CV), X-ray diffraction (XRD), and X-ray photoelectron spectroscopy (XPS). XRD data in Fig. 1b and SEM images in Fig. 1c demonstrate that film is obtained as a nanostructured film, with CoP as the dominant phase. Surface area grazing incidence XRD spectra for a Co-PP film on Ni and a Co-PP powder prepared from commercial  $\text{Co}_3\text{O}_4$ <sup>†</sup> are shown in Fig. 1b. These patterns indicate the formation of CoP (PDF# 00-029-0497) as the major phase of cobalt phosphide. This first unassigned peak ( $\sim 41^\circ 2\theta$ ) can be assigned to either an alternate, minor cobalt phosphide phase,  $\text{Co}_2\text{P}$  (PDF# 01-072-9563), or a nickel or cobalt/nickel phase that has formed at the substrate surface,  $\text{Ni}_2\text{P}$  (PDF# 01-072-2514) or  $\text{NiCoP}$  (PDF# 01-071-2336), respectively. The second unassigned, broad peak ( $\sim 65^\circ 2\theta$ ) is associated with the spinel cobalt oxide, likely residual  $\text{Co}_3\text{O}_4$  from the precursor film that was not fully converted to phosphide. The

highly textured, nanostructured features obtained with the initial  $\text{Co}(\text{NO}_3)_x(\text{OH})_{2-x}\cdot y(\text{H}_2\text{O})$  film that are known to be retained upon conversion to  $\text{Co}_3\text{O}_4$ ,<sup>8</sup> are further retained in the Co-PP film, as shown in Fig. 1c.

The benefits of a nanostructured electrocatalyst film without additives such as carbon (potentially suffering corrosion at OER potentials) or polymer (potentially interfering with mass transport) was recently demonstrated for  $\text{Co}_3\text{O}_4$ -based films as bifunctional catalysts for oxygen electrochemistry.<sup>8</sup> Electrodeposition provides for direct contact of the film with the substrate resulting in excellent mechanical adhesion and electron transfer between the current collector and the film. Additionally, virtually any conductive substrate can be used provided it is compatible with further processing conditions. The formation of a nanostructured, porous film provides a high surface area upon which the catalytic reaction occurs, as well as for more facile ion transport.

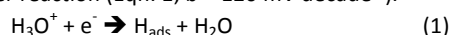
The electrochemically active surface area (ECSA) of the Co-PP film was then determined by CV, as previously described (Fig. S2 (ESI<sup>†</sup>)).<sup>8</sup> Using an estimated specific capacitance value<sup>14</sup> of 40  $\mu\text{F cm}^{-2}$ , the ECSA of the Co-PP film is 33.1  $\text{cm}^2$ , with a roughness factor (RF) of 169. This is higher than the previously reported RF value of 95 for a similar cobalt phosphide/phosphate thin film;<sup>14</sup> however, these differences may be due to variances in surface composition between the two films (i.e. phosphide versus phosphate content and their effect on capacitance).

Due to its high surface area, reaction of Co-PP films with oxygen is expected upon exposure to air.<sup>25</sup> This presence of a surface phosphate species rationalizes the efficient OER activity of the Co-PP films.<sup>26</sup> XPS data is shown in Fig. 1d. The Co 2p spectra peaks at  $\sim 778$  eV and 793 eV associate with CoP (and possibly metallic Co).<sup>25</sup> The expected phosphate and other oxidized species of Co ( $\text{Co}_3\text{O}_4$ , also probable in XRD), appear at  $\sim 782$  eV and 797 eV.<sup>25</sup> The peak at 134 eV in the P 2p spectra confirms the presence of a phosphate species. This peak compares very closely to a  $\text{Co}_3(\text{PO}_4)_2$  salt as previously reported.<sup>9</sup> The “shoulder” appearance of the 130 eV peak in the P 2p region is likely an overlap of the  $2p_{1/2}$  and  $2p_{3/2}$  states of CoP. For more information on the phosphide-phosphate relationship, the reader is directed to the studies of Yang *et al.*<sup>14</sup> and Jiang *et al.*<sup>15</sup> In summary, these studies showed that the phosphide: phosphate ratio changed at different film depths,<sup>14</sup> and subjecting the film to oxidizing and reducing potentials changed the phosphide: phosphate ratio.<sup>15</sup> As would be expected, the phosphate concentration increases at the surface of the film, and after being run at highly positive (OER) potentials, while the phosphide species concentration increases at the base of the film, and after being run at highly negative (HER) potentials.<sup>14-15</sup>

The Co-PP films were then evaluated for their ability to act as electrocatalysts for the HER in 0.5 M  $\text{H}_2\text{SO}_4$  and 0.1 M KOH electrolytes, by rotating disk voltammetry (RDV) (Fig. 2). From the outset it was expected that Ti would be the most suitable and practical substrate for acidic conditions, while Ni would be preferred under alkaline conditions. Au<sup>†</sup> was also examined as it was expected to be electrochemically inert/stable under both conditions. Control experiments of Ni, Ti, and Au substrates and substrates exposed to the low temperature phosphidation reaction ( $\text{Ni}^*$ ,  $\text{Ti}^*$ , and  $\text{Au}^*$ )<sup>†</sup> can be found in Fig. S3 and Fig. S4 (ESI<sup>†</sup>).

Fig. 2a demonstrates that Co-PP is quite active for the HER in acid (0.5 M H<sub>2</sub>SO<sub>4</sub>) on each substrate (hereby termed Co-PP/substrate), with each sample exhibiting potentials only 0.109 to 0.127 V more negative than 20% Pt/C, at any given current density (*j*<sub>geo</sub>) value. HER effectiveness, as determined from the voltage observed at -10 mA cm<sup>-2</sup>, was found to be in the order of: 20% Pt/C (-0.056 V) > Co-PP/Ti (-0.165 V) > Co-PP/Ni (-0.171 V) > Co-PP/Au (-0.183 V). A precursor Co<sub>3</sub>O<sub>4</sub> film was also tested for the HER. Its poor HER activity proves that the precursor Co<sub>3</sub>O<sub>4</sub> is not a HER-OER bifunctional catalyst (although shown to exhibit ORR-OER bifunctionality<sup>8</sup>), necessitating the conversion to cobalt phosphide/phosphate (Fig. S5, ESI<sup>†</sup>). Stability tests in 0.5 M H<sub>2</sub>SO<sub>4</sub> were conducted with repetitive RDV scans and the pertinent data is shown in Fig. 2b. The data demonstrates that both Co-PP/Ti and Co-PP/Au are quite stable under repetitive HER scans, with Co-PP/Ti degrading by ~30 mV, and Co-PP/Au improving by ~10 mV (again, as measured by the voltage change between cycle 1 and cycle 100, at -10 mA cm<sup>-2</sup>). The HER activity of Co-PP/Ni declines significantly, despite its good mechanical adhesion throughout the study. While a continuous film is formed (on all substrates), the porous nature likely allows for some solubility of the Ni substrate during testing in acidic conditions. In the series here, the earliest onset potential values under acidic conditions were found to be Co-PP/Ti (-0.075 V) ~ Co-PP/Ni (-0.076 V) > Co-PP/Au (-0.091 V). Onsets were determined using a tangential method and likely underestimate the value as compared to literature values.<sup>‡</sup> A total comparison shows that Ti is the best substrate for supporting the Co-PP film in acidic conditions.

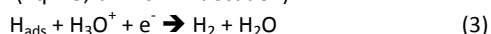
The Tafel slope (b) is a useful metric of comparison in both acidic and alkaline electrolyte, representing a material's ability to respond to a potential change and generate current. The Tafel slope is especially useful in acidic media, as the acidic HER mechanisms are well known.<sup>27</sup> The HER proceeds, first, by the surface adsorption of a proton, the Volmer reaction (Eqn. 1; b = 120 mV decade<sup>-1</sup>).



However, the subsequent step is known to differ, and can be differentiated by the Tafel slope. The HER can either proceed by a recombination of two adsorbed protons (H<sub>ads</sub>), the Tafel reaction (Eqn. 2; b = 30 mV decade<sup>-1</sup>);



Or by the electrochemical desorption of a surface proton, the Heyrovsky reaction (Eqn. 3; b = 40 mV decade<sup>-1</sup>).



Pt and Pt/C catalysts are known to proceed by the Volmer-Tafel mechanism, which is confirmed here by the obtained slope of 32 mV decade<sup>-1</sup>, Fig. 2c. The values for the Co-PP film electrocatalysts in Fig. 2c suggest that they all proceed by the Volmer-Heyrovsky mechanism in 0.5 M H<sub>2</sub>SO<sub>4</sub>: 59, 60, and 69 mV decade<sup>-1</sup> for Co-PP/Au, Co-PP/Ni, and Co-PP/Ti, respectively.

The HER was also tested in 0.1 M KOH. The HER is known to be more difficult in alkaline electrolyte, requiring much higher overpotentials to achieve current densities comparable to acidic electrolyte. This phenomena is shown by the more positive voltages observed for Pt/C to reach -10 mA cm<sup>-2</sup>, i.e. -0.056 V in 0.5 M H<sub>2</sub>SO<sub>4</sub> versus -0.165 V in 0.1 M KOH. Voltages at -10 mA cm<sup>-2</sup> for all of the Co-PP films were ~ 0.129-0.412 V more negative in value. The order of activity among the Co-PP films is now reversed, with overall

activity: 20% Pt/C (-0.165 V) > Co-PP/Au (-0.312 V) > Co-PP/Ni (-0.411 V) > Co-PP/Ti (-0.577 V) at 10 mA cm<sup>-2</sup> (Fig. 2d).

Repetitive RDV data shown in Fig. 2e demonstrates excellent stability for all films under these conditions, with less than 10 mV losses in all cases. Tafel slopes were once again calculated (Fig. 2f), to compare catalytic activity in alkaline electrolyte. Similar trends are seen, with the Tafel slopes in the range of 2-3 times higher than that of 20% Pt/C. Tafel slopes in alkaline electrolyte are generally higher for all materials, as the Volmer reaction becomes more rate determining. This could be attributed to differing surface features that perform hydrogen adsorption and desorption in alkaline versus acidic electrolyte.<sup>1</sup> The Co-PP/Au catalyst in particular, which demonstrated high activity in 0.1 M KOH by RDV, also has one of the lowest alkaline Tafel slopes [100 mV decade<sup>-1</sup> in 0.1 M KOH, 67 mV decade<sup>-1</sup> in 1 M KOH (Fig. S6, ESI<sup>†</sup>)] so far reported in the literature for similar catalysts,<sup>1,12-13</sup> see Table S1 (ESI<sup>†</sup>).

OER performance in 0.1 M KOH for all films demonstrates that Co-PP/Ni and Co-PP/Au outperform that of Co-PP/Ti (Fig. 3a). Onset potential<sup>‡</sup> values were determined to be ~ 1.59 V (Co-PP/Ni and Co-PP/Au) versus 1.62 V (Co-PP/Ti). Voltages at 10 mA cm<sup>-2</sup> are routinely reported as an OER metric due to its relevance for solar fuels synthesis.<sup>28</sup> Trends here are Co-PP/Ni (1.72 V) > Co-PP/Au (1.74 V) > Co-PP/Ti (1.94 V) >> 20% Pt/C (did not reach 10 mA cm<sup>-2</sup> in our hands).<sup>‡</sup> Fig. 3b shows normalized galvanostatic data at 10 mA cm<sup>-2</sup> for 2 h, demonstrating the stable OER performance of both Co-PP/Ni (< 1 %) and Co-PP/Au (< 1 % loss), and the degradation and poorer performance of Co-PP/Ti (~ 9 % loss) and 20% Pt/C (~ 26 % loss).

Considering the excellent HER and OER performance with Co-PP/Au in 0.1 M KOH solution, it was then tested in 1 M KOH to allow for a more direct comparison to recent, similar studies.<sup>12-14</sup> Fig. 3c shows HER and OER RDV scans of Co-PP/Au in 1 M KOH, with decreased overpotentials (η) as compared to 0.1 M KOH at the HER and OER metric current density values of -10 and 10 mA cm<sup>-2</sup>, respectively. Specifically, the HER η values improved from -0.305 V (0.1 M KOH) to -0.196 V (1.0 M KOH), while the OER values improved from 1.74 V (0.1 M KOH) to 1.57 V (1 M KOH). In fact, Co-PP/Au performs very well when compared, particularly on an equivalent mass loading basis, to other state-of-the-art HER-OER bifunctional electrocatalysts in 1 M KOH electrolyte (Table S1, ESI<sup>†</sup>).

The ability of Co-PP films to catalyze the HER and OER effectively suggest they could serve as both the anode and cathode in an electrolyzer, or serve as bi-directional electrodes in regenerative fuel cells.<sup>3</sup> A symmetrical electrolysis cell was constructed with Co-PP/Au at both the anode and cathode in a two-electrode system for the following experiments, as pictured in Fig. 3f. First, a positive RDV scan past the theoretical reversible potential of OER/HER @ 1.23 V, to 2 V, showed an early onset potential and significant current and gas formation at each electrode (Fig. 3d). 10 mA cm<sup>-2</sup> was once again chosen as the current to examine the device's stability over a two-hour period (Fig. 3e). Gas accumulation on the catalyst surface was observed, so care was taken to remove bubbles (which can increase the operating voltage due to transport-related resistances) when formed. With this in mind, the galvanostatic experiment in Fig. 3e shows excellent stability over two hours (< 5 mV change). The voltage increase from the RDV scan to constant electrolysis is likely

due to unavoidable gas accumulation on the electrode: initial RDV scan ( $\eta = 0.41$  V – dotted line, Fig. 3d), to beginning of the stability test ( $\eta = 0.49$  V) to the end ( $\eta = 0.51$  V). This cell overpotential is among the lowest of the reported Co-based catalyst symmetrical electrolysis cells in the literature, and at a much lower mass loading (Table S1, ESI†).<sup>10, 12-15</sup>

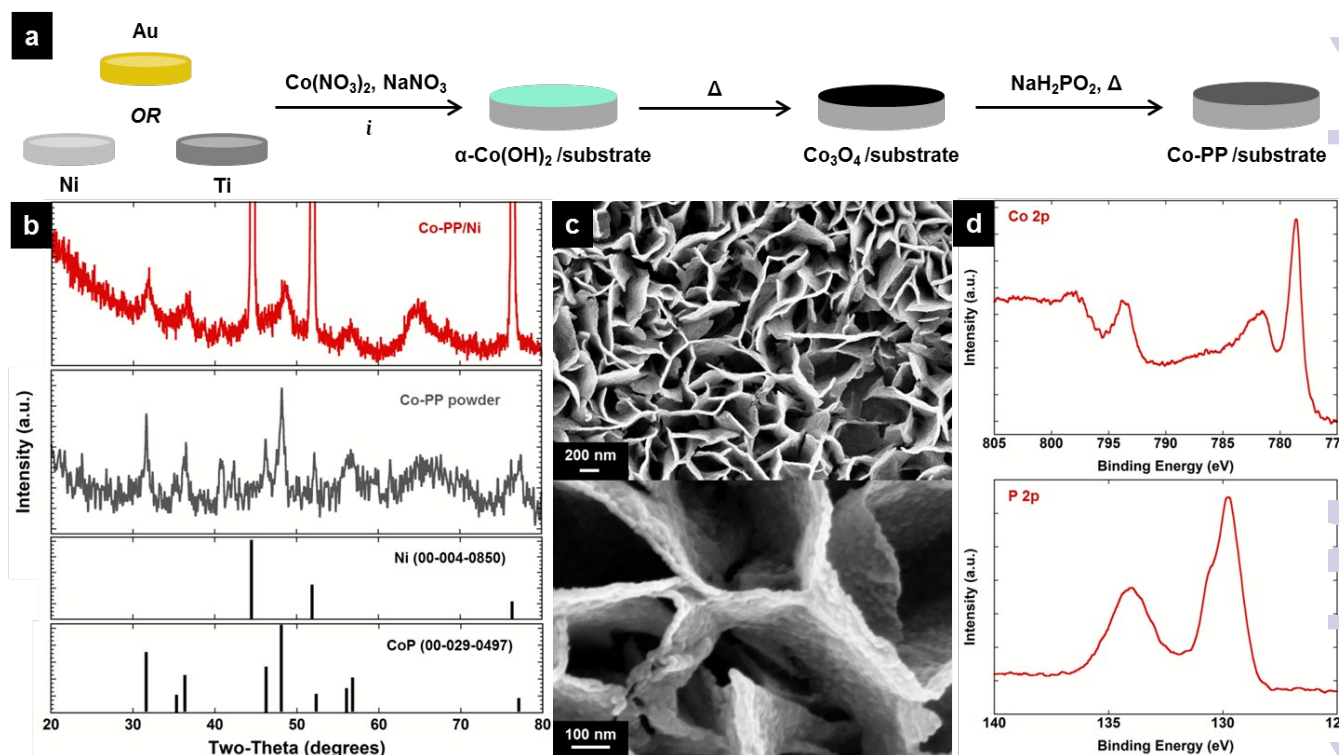
In conclusion, nanostructured, high surface area Co-PP films have been prepared by an electrodeposition-thermal annealing-phosphidation method on several conductive substrates. The Co-PP films performed well as electrocatalysts for the HER, in both acidic ( $\eta = 0.165 - 0.183$  V @  $-10$  mA cm<sup>-2</sup>) and alkaline ( $\eta = 0.196 - 0.577$  V @  $-10$  mA cm<sup>-2</sup>) electrolyte, and OER in alkaline electrolyte ( $\eta = 0.34 - 0.71$  V @  $10$  mA cm<sup>-2</sup>). This bifunctional activity is attributed to the nanostructured, high surface area and stability over a wide pH range. A symmetrical electrolysis cell using Co-PP at each electrode was assembled and provided low cell overpotentials ( $\eta = 0.41 - 0.51$  V) for water electrolysis. The success of these films augurs for additional development of bifunctional HER-OER electrocatalysts.

This work was supported by the Laboratory Directed Research and Development program at Sandia National Laboratories, a multi-program laboratory managed and operated by Sandia Corporation, a wholly owned subsidiary of Lockheed Martin Corporation, for the U.S. Department of Energy's National Nuclear Security Administration under contract DE-AC04-94AL85000. Dr. Michael Brumbach, Ms. Bonnie McKenzie, Dr. Mark Rodriguez, and Ms. Suzanne White are thanked for their technical assistance.

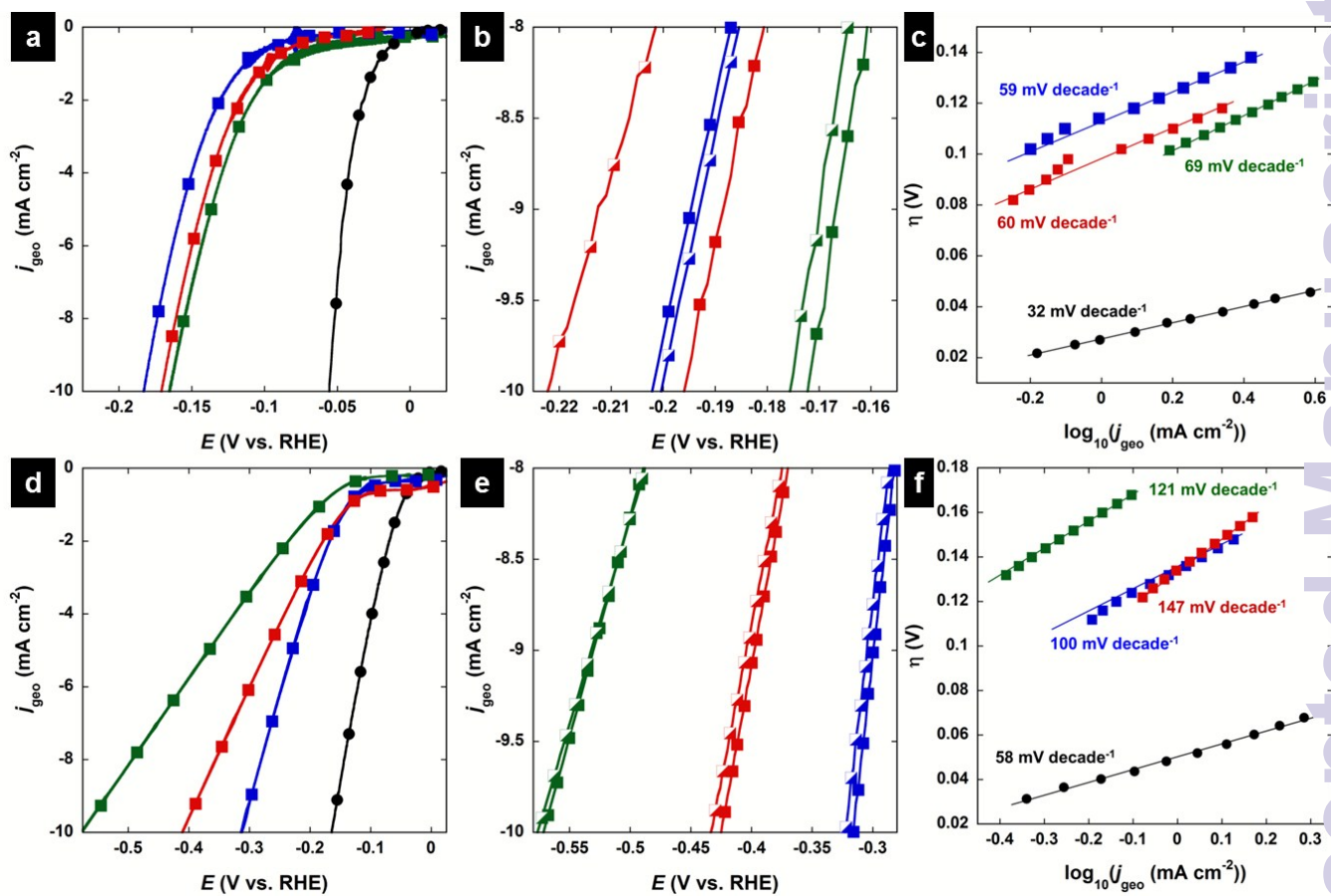
## Notes and references

† Further details are described in the ESI: Au foil refers to the use of Au-sputtered Ni foil; Onset potentials were calculated by the tangential method.; 20% Pt/C was newly purchased. Attempts to activate the Pt/C in reducing atmospheres failed to increase the activity.

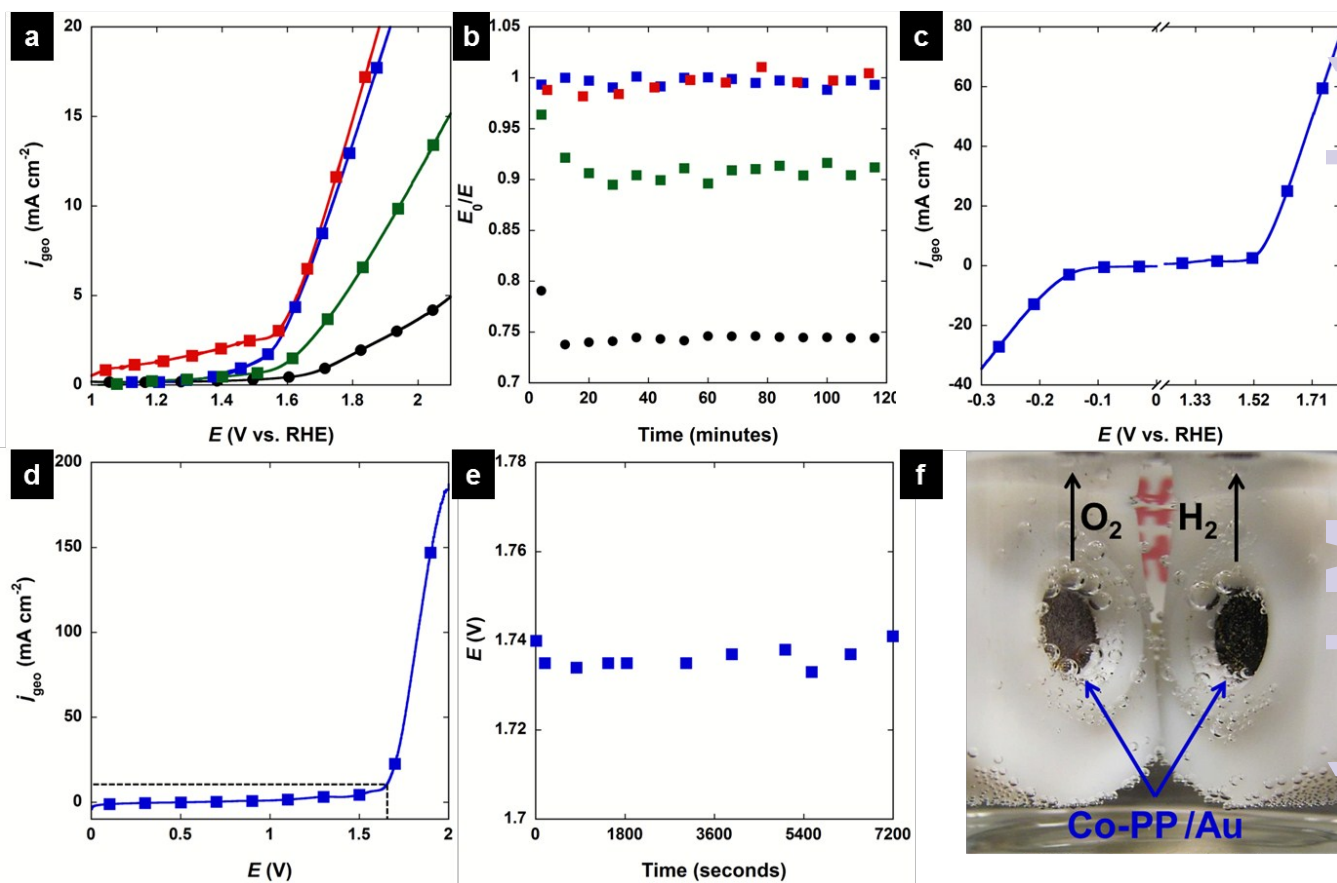
- 1 K. Zeng and D. Zhang, *Prog. Energ. Combust.*, 2010, **36**, 307-326.
- 2 A. J. Bard and M. A. Fox, *Accounts Chem. Res.*, 1995, **28**, 141-145.
- 3 J. Ahn and R. Holze, *J. Appl. Electrochem.*, 1992, **22**, 1167-1174.
- 4 M. G. Walter, E. L. Warren, J. R. McKone, S. W. Boettcher, Q. Mi, E. A. Santori and N. S. Lewis, *Chem. Rev.*, 2010, **110**, 6446-6473.
- 5 C. G. Morales-Guio, L.-A. Stern and X. Hu, *Chem. Soc. Rev.*, 2014, **43**, 6555-6569.
- 6 J. F. Callejas, C. G. Read, E. J. Popczun, J. M. McEnaney and R. E. Schaak, *Chem. Mater.*, 2015, **27**, 3769-3774.
- 7 E. J. Popczun, C. G. Read, C. W. Roske, N. S. Lewis and R. E. Schaak, *Angew. Chem.*, 2014, **126**, 5531-5534.
- 8 T. N. Lambert, J. A. Vigil, S. E. White, D. J. Davis, S. J. Limmer, P. D. Burton, E. N. Coker, T. E. Beechem and M. T. Brumbach, *Chem. Commun.*, 2015, **51**, 9511-9514.
- 9 S. Cobo, J. Heidkamp, P.-A. Jacques, J. Fize, V. Fourmond, L. Guetaz, B. Jousset, V. Ivanova, H. Dau, S. Palacin, M. Fontecave and V. Artero, *Nat. Mater.*, 2012, **11**, 802-807.
- 10 J. Wang, D. Gao, G. Wang, S. Miao, H. Wu, J. Li and X. Bao, *J. Mater. Chem. A*, 2014, **2**, 20067-20074.
- 11 H. Lei, A. Han, F. Li, M. Zhang, Y. Han, P. Du, W. Lai and R. Cao, *Phys. Chem. Chem. Phys.*, 2014, **16**, 1883-1893.
- 12 H. Jin, J. Wang, D. Su, Z. Wei, Z. Pang and Y. Wang, *J. Am. Chem. Soc.*, 2015, **137**, 2688-2694.
- 13 S. Du, Z. Ren, J. Zhang, J. Wu, W. Xi, J. Zhu and H. Fu, *Chem. Commun.*, 2015, **51**, 8066-8069.
- 14 Y. Yang, H. Fei, G. Ruan and J. M. Tour, *Adv. Mater.*, 2015, **27**, 3175-3180.
- 15 N. Jiang, B. You, M. Sheng and Y. Sun, *Angew. Chem. Int. Ed.*, 2015, **54**, 6251-6254.
- 16 H. Wang, H.-W. Lee, Y. Deng, Z. Lu, P.-C. Hsu, Y. Liu, D. Lin and Y. Cui, *Nat. Commun.*, 2015, **6**.
- 17 H. Zhu, J. Zhang, R. Yanzhang, M. Du, Q. Wang, G. Gao, J. Wu, G. Wu, M. Zhang, B. Liu, J. Yao and X. Zhang, *Adv. Mater.*, 2015, **27**, 4752-4759.
- 18 Q. Li, Z. Xing, A. M. Asiri, P. Jiang and X. Sun, *Int. J. Hydrogen Energ.*, 2014, **39**, 16806-16811.
- 19 M. Li, X. Liu, Y. Xiong, X. Bo, Y. Zhang, C. Han and L. Guo, *J. Mater. Chem. A*, 2015, **3**, 4255-4265.
- 20 Q. Liu, J. Tian, W. Cui, P. Jiang, N. Cheng, A. M. Asiri and X. Sun, *Angew. Chem. Int. Ed.*, 2014, **53**, 6710-6714.
- 21 J. Tian, Q. Liu, A. M. Asiri and X. Sun, *J. Am. Chem. Soc.*, 2014, **136**, 7587-7590.
- 22 S. Gu, H. Du, A. M. Asiri, X. Sun and C. M. Li, *Phys. Chem. Chem. Phys.*, 2014, **16**, 16909-16913.
- 23 H. Du, Q. Liu, N. Cheng, A. M. Asiri, X. Sun and C. M. Li, *J. Mater. Chem. A*, 2014, **2**, 14812-14816.
- 24 Q. Guan and W. Li, *J. Catal.*, 2010, **271**, 413-415.
- 25 F. H. Saadi, A. I. Carim, E. Verlage, J. C. Hemminger, N. S. Lewis and M. P. Soriaga, *J. Phys. Chem. C*, 2014, **118**, 29294-29300.
- 26 Y. Surendranath, M. W. Kanan and D. G. Nocera, *J. Am. Chem. Soc.*, 2010, **132**, 16501-16509.
- 27 Y. Li, H. Wang, L. Xie, Y. Liang, G. Hong and H. Dai, *J. Am. Chem. Soc.*, 2011, **133**, 7296-7299.
- 28 C. C. L. McCrory, S. Jung, J. C. Peters and T. F. Jaramillo, *J. Am. Chem. Soc.*, 2013, **135**, 16977-16987.



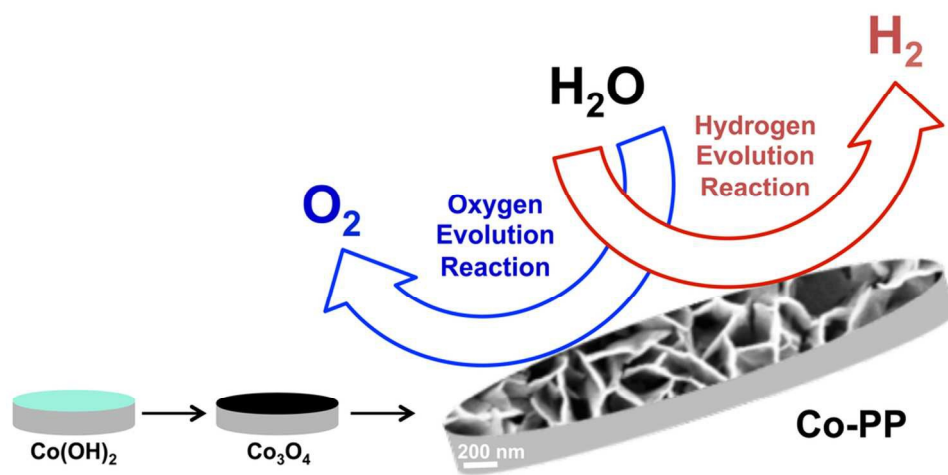
**Fig. 1** (a) Electrodeposition-thermal annealing-phosphidation reaction schematic on Ni, Ti, and Au foil substrates; (b) XRD spectra of Co-PP/Ni and Co-PP powder indexed to Ni (PDF #00-004-0850) and CoP (PDF #00-029-0497); (c) SEM images of Co-PP/Ni; (d) XPS spectra of Co-PP/Ni, in the Co 2p (top) and P 2p (bottom) regions.



**Fig. 2** HER experiments performed in (a)-(c) 0.5 M H<sub>2</sub>SO<sub>4</sub> or (d)-(f) 0.1 M KOH. (a,d) RDV scans of Co-PP/Ni (red, filled squares), Co-PP/Ti (green, filled squares), Co-PP/Au (blue, filled squares), and 20% Pt/C (black, filled circles); (b,e) RDV Stability of Co-PP/Ni, Co-PP/Ti, and Co-PP/Au, cycle 1 (filled squares) vs. cycle 100 (half-open squares); (c,f) Tafel plot and slopes of Co-PP/Ni, Co-PP/Ti, Co-PP/Au, and 20% Pt/C.



**Fig. 3** (a),(b) OER experiments done in 0.1 M KOH, (c)-(f) Electrolysis experiments done in 1 M KOH. (a) RDV scans of Co-PP/Ni (red, filled squares), Co-PP/Ti (green filled squares), Co-PP/Au (blue, filled squares), and 20% Pt/C (black, filled circles); (b) Galvanostatic stability of Co-PP/Ni, Co-PP/Ti, Co-PP/Au, and 20% Pt/C at  $j_{geo} = 10 \text{ mA cm}^{-2}$  for 2 hours; (c) HER and OER RDV scans of Co-PP/Au; (d) RDV scan, dotted line marks  $j_{geo} = 10 \text{ mA cm}^{-2}$ ; (e) galvanostatic stability at  $j_{geo} = 10 \text{ mA cm}^{-2}$  for hours; (f) image of electrolysis cell assembly.



95x48mm (300 x 300 DPI)